The role of Pt addition on the photocatalytic activity of TiO$_2$ nanoparticles: The limit between doping and metallization

Adriane V. Rosario, Ernesto C. Pereira*

Laboratório Interdisciplinar de Eletroquímica e Cerâmica, Centro Multidisciplinar para o Desenvolvimento de Materiais Cerâmicos, Departamento de Química, Universidade Federal de São Carlos, P.O. Box 676, 13565-905 São Carlos, SP, Brazil

A B S T R A C T

Platinum-loaded titanium oxide nanoparticles, Pt-TiO$_2$, were prepared using the polymeric precursor method with titanium isopropoxide as metal precursor. Platinum ions were added to the titanium precursor solution with Pt/Ti molar ratios between 0.005 and 10 mol%. The characterization of the physical properties was carried out by BET-surface area, transmission electron microscopy (TEM) and X-ray diffraction (XRD) with Rietveld quantitative analysis. The XRD patterns indicated that Pt doping occurred only for samples containing less than 1.0 mol% of platinum, and a small amount of rutile phase was observed after doping. For 1.0 mol% or higher Pt concentration a metallic Pt phase was detected. On the other hand, TEM analysis showed that the doping/metallization limit is still lower. Samples with nominal Pt concentration of 0.1 mol% presented signal of Pt metal particles. The photocatalytic activities of the samples were studied using methyl orange (MO) as model compound under UV illumination. In all Pt-TiO$_2$ samples the photocatalytic activity was found to increase in comparison with pure TiO$_2$ samples, either by the doping mechanism (at a low Pt concentration level), or by charge transfer mechanism in the interface metal/oxide (at a high Pt concentration level). The increase in Pt content, up to 0.2 mol% of Pt, was found to enhance the photocatalytic activity of TiO$_2$ towards the decomposition of MO. At even higher concentrations, platinum no longer acted as a dopant: instead, metallic Pt particles decorated the oxide surface. Doped and metallized samples had similar photocatalytic activity.

© 2013 Elsevier B.V. All rights reserved.

1. Introduction

Photocatalytic reactions based on semiconductors, as TiO$_2$, are initiated by light absorption, in this case in the UV range. UV radiation absorption leads to the excitation of electrons (e$^-$) from the valence band (VB) to the conduction band (CB), producing positive charge carriers, holes (h$^+$), in the valence band, as reproduced in Equation 1 according to Kröger–Vink notation (e$^-$ and h$^+$ are represented by a negative e′ and a positive defect O$_O^\bullet$, respectively):

$$TiO_2 + h\nu \rightarrow e' + Ti_{Ti}^x + O_O^\bullet + O_O^x \qquad (1)$$
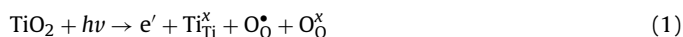
Both charge carriers, e$^-$ and h$^+$, migrate to the TiO$_2$ surface acting as reduction or oxidation sites, respectively. However, the use of TiO$_2$ as photocatalyst has important challenges, once the quantum efficiencies of photo-induced processes are very low. This occurs due to photocatalytic reaction rates are not fast enough to compete with the charge carrier recombination. As a consequence, in the last years, most of the published papers directed their attention towards the synthesis of TiO$_2$ with improved properties. It is well established that the activity of TiO$_2$ depends on its surface and bulk properties in addition to, of course, the nature of the substrate to be degraded. In this sense, during the last decade different methods for producing TiO$_2$ have been employed, such as chemical vapour deposition (CVD) [1–3], metal organic chemical vapour deposition (MOCVD) [4,5], sputtering [6–8], pyrolysis [9,10], sol–gel processes [11–14], anodic oxidation [15–20], and hydrothermal synthesis [21,22].

Moreover, different strategies have been used to improve TiO$_2$ photocatalytic activity such as deposition over other materials, dye sensitization, doping and metallization. Among these strategies, doping and metallization are the main used procedures. It has been reported that doping with different transition metal ions can lead to an enhancement in the photocatalytic activity of TiO$_2$ as this process extends the sample's light absorption to the visible region. Different chemical elements have been proposed to dope TiO$_2$, either metals, such as Fe, W, Nb, or non-metals, such as N, C and S. The latter case, non-metals are used to replace oxygen atoms in the lattice. This effect has been reviewed by Carp et al. [23] and Rehman et al. [24]. However, the explanation of the results about photocatalytic efficiency variation is still controversial. Different structural and morphological changes depend on the preparation

method and dopant concentration, resulting in positive or negative influences on the photocatalytic properties. Indeed, doping ions can also change the life time of the charge carriers, since they act as trapping sites, promoting the e^-/h^+ recombination.

In the metallization case, TiO_2 photocatalysts are modified with nanoparticles of noble metals such as Ag, Au, and Pt deposited on the particles surface [25–31]. In this case, it is proposed that the metal/TiO_2 heterojunction influences the charge transfer process over the semiconductor particles. The difference between the work function of the metal islands and the Fermi level of TiO_2 results in the formation of a Schottky barrier between these components. With irradiation, the electrons in the conduction band flow from TiO_2 particles to the metal, increasing the charge separation and, consequently, decreasing the e^-/h^+ recombination. Additionally, electrons trapped on the metal surface can also act as reduction centres for adsorbed species. Usually, photodeposition has been used to decorate TiO_2 particles [29–31].

In the last years, Pt-modified TiO_2 are being investigated mainly under visible light irradiation [32–35], and although there are several studies regarding Pt-coated TiO_2 catalysts, Pt-doped TiO_2 samples have not been deeply studied. Currently, platinum is one of the most applied metals to enhance the photocatalytic properties of TiO_2. However, it is important to stress out that there is some confusion in the literature due the incorrect use of the term "doping". In most of the cases, TiO_2 decorated with Pt nanoparticles are called "doped systems". In fact, such term can only be employed if Pt ions are incorporated into the oxide matrix, replacing Ti^{4+} ions, or eventually, in interstitial sites. In this sense, Kim et al. [36] studying Pt_{ion}-doped TiO_2 at doping levels ranging from 0.2 to 2.0 at%, observed noticeable differences in the photocatalytic properties when these samples are compared to Pt-metal-loaded TiO_2. Choi et al. [35] prepared TiO_2 samples doped with 13 different metal ions, among then Pt^{2+} and Pt^{4+}. The authors confirmed the substitution of Ti^{4+} by Pt ions through elemental composition analysis by energy dispersive X-ray spectroscopy and observed significant enhanced visible-light photoactivity for decomposition of methylene blue, iodide and phenol.

In this context, this paper presents a systematic study of the effect of Pt-loading composition on photocatalytic properties. We have used the polymeric precursor method as an alternative synthesis route with the purpose of evaluating the effect of Pt content variation. This experimental procedure enables not only to control the concentration of Pt, working with very low doping levels, but also, permits the obtainment of samples decorated with Pt-metal maintaining the characteristics of oxide preparation. Thus, in this one-step synthesis, the effects observed on the photocatalytic properties of TiO_2 can be directly related only to the addition of platinum, eliminating other preparation variable effects. Finally, we corroborate this with evidence about the correlation between doping and photoactivity enhancement, which depends on the solubility limit of platinum metal ions in the TiO_2 matrix.

2. Experimental

2.1. Sample preparation

Pt-doped TiO_2 powders were prepared according to the process shown in Fig. 1, using citric acid (Synth p.a.), ethylene glycol (Mallinckrodt) and as metal precursors, titanium IV isopropoxide (Alfa Aeser) and hexachloroplatinic acid (Sigma–Aldrich). The precursor solutions were prepared by dissolving titanium IV isopropoxide and hexachloroplatinic acid in ethylene glycol under vigorous stirring at 70 °C. After this, the citric acid was added while stirring and heat were maintained until the complete dissolution of the citric acid. Precursor solutions were prepared in the following
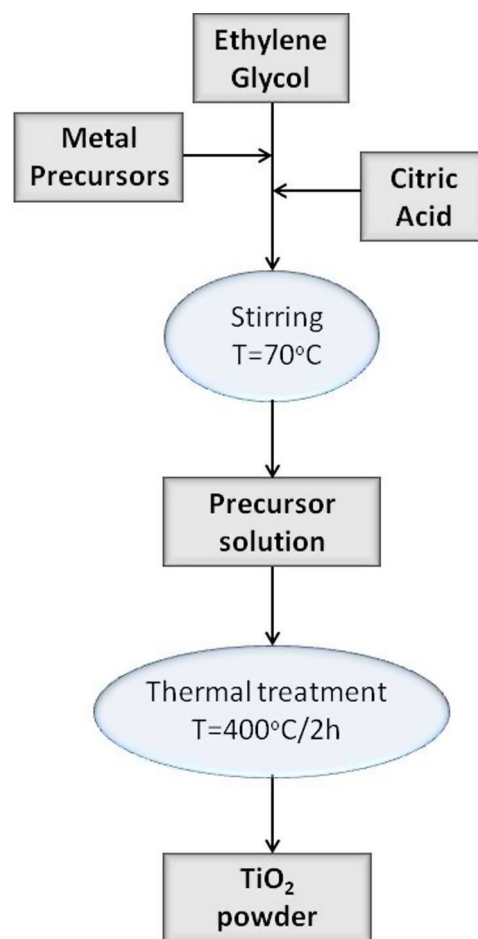

Fig. 1. Schematic representation of the preparation process of the Pt-TiO_2 powders.

rate: titanium IV isopropoxide: citric acid: ethylene glycol 1:8:32, which was loaded with different Pt ions concentrations; between 0.005% and 10 mol%. Subsequently, the precursor solutions were submitted to thermal treatment at 400 °C for 2 h to promote the elimination of organic part and oxidation of the metal. Fine powders were obtained by grinding TiO_2 samples after calcination.

2.2. Photocatalytic experiments

The experiments were performed in a box photoreactor equipped with six UV lamps of $\lambda = 253.7$ nm (Phillips – 15 W). The experiments were conducted in an open glass vessel surrounded by a water circulating jacket to maintain the thermostatized temperature at 20 °C. The substrate was a 6×10^{-5} mol L^{-1} methyl orange (MO) aqueous solution at pH = 3. This compound has a maximum absorption at 508 nm. For each photocatalytic run, 50 mg of TiO_2 powder was added to 50 mL of MO solution. The suspension was maintained under stirring and in the dark for 30 min (for the dye adsorption on the oxide particles surface). After this, the irradiation was started and solution aliquots were collected every 10 min. The samples were immediately centrifuged to separate the TiO_2 and the analysis of MO concentration in the reaction products was carried out by spectrophotometry using a UV–vis–NIR spectrophotometer (Cary model 5G). Previously, a calibration plot based on the Lambert–Beer law was established, relating the absorbance to the concentration. The maximum absorbance of the MO solution was used to determine the concentration of the collected aliquots.
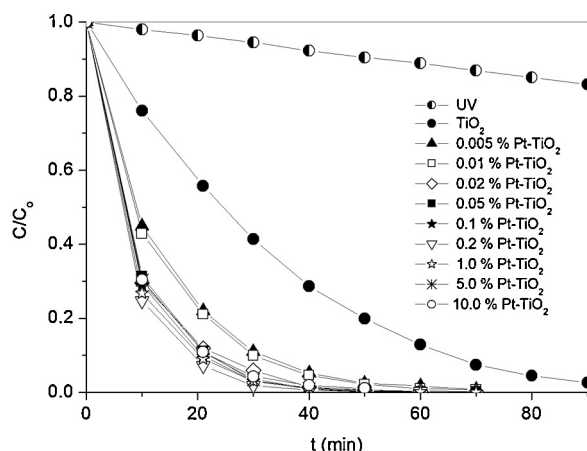
Fig. 2. MO concentration change versus irradiation time for UV without catalyst, and UV in the presence of pure TiO_2 and Pt-loaded TiO_2 nanoparticles. $T = 25\,°C$.
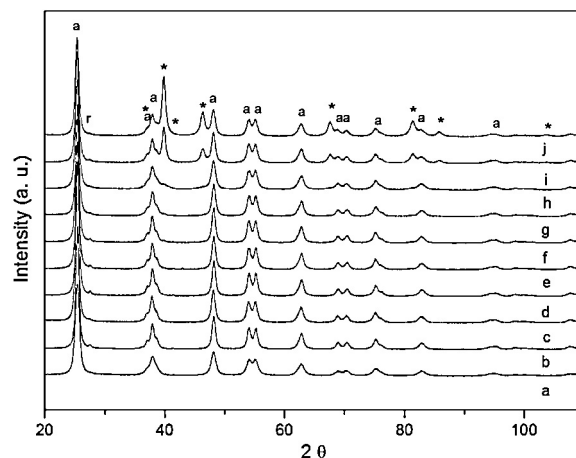

Fig. 3. XRD patterns of samples: (a) pure TiO_2, (b) (Pt 0.005%)TiO_2, (c) (Pt 0.01%)TiO_2, (d) (Pt 0.02%)TiO_2, (e) (Pt 0.05%)TiO_2, (f) (Pt 0.1%)TiO_2, (g) (Pt 0.2%)TiO_2, (h) (Pt 1.0%)TiO_2, (i) (Pt 5.0%)TiO_2, and (j) (Pt 10.0%)TiO_2.

2.3. Physical characterization

The powders were analysed by X-ray diffraction with a diffractometer (Rigaku model DMax/2500PC), using Cu Kα radiation ($\lambda = 1.54\,\text{Å}$). The diffractograms were obtained in the 2θ range between $20°$ and $110°$ with a step of $0.05°$ and a measuring time of 0.5 s per point. The General Structure Analysis System (GSAS) program was used to analyse the XRD data by the Rietveld refinement method [37]. Transmission electron microscopy (TEM) was performed in a Philips CM200 microscope operating at 200 kV. BET surface areas were determined by the physical adsorption of N_2 using an ASAP2000 equipment.

3. Results and discussion

Sample catalyst activities were evaluated using methyl orange as a model compound as described in the Experimental section. Fig. 2 presents concentration as a function of discoloration time. UV irradiation without catalysts leads to a small decrease in the 508 nm band, which is used to follow the dye concentration decrease: 5% for 30 min of reaction. This figure shows also that the addition of platinum resulted in an enhancement of photocatalytic activity comparing with pure TiO_2 sample. The apparent rate constants, k, were calculated from the slope of the $\ln(C/C_0)$ versus time and results are presented in Table 1. Besides, it was observed that the linear correlation coefficients were higher than 0.98, which is in agreement with a pseudo-first-order kinetics.

These results were compared with P25® (Degussa) TiO_2 commercial sample under the same analysis conditions. P25 is composed of 80% anatase phase and 20% rutile phase, with an

average crystallite size for the anatase phase of 22 nm and a specific surface area of $50\,m^2\,g^{-1}$. The pure TiO_2 sample prepared using the polymeric precursor method showed similar behaviour to P25, although the area and composition were different. The results indicate that the rate constant increased as Pt content increased up to 0.2 mol%, and then slightly decreased for higher Pt amounts, suggesting a critical limit of Pt content. However, even for high Pt content, k values remained higher than those observed for doped TiO_2 with low Pt level (0.02–0.05 mol%). These results attests that it is possible to obtain the same efficiency for the dye degradation using small Pt amounts, differently than the usual approach which has been extensively proposed by the use of platinized TiO_2 photocatalysts.

The specific surface areas of the catalysts are also shown in Table 1. The surface area calculated, using BET isotherm, S_{BET}, ranged between 48 and $84\,m^2\,g^{-1}$. For most of the samples, Pt load led to a decrease in the active area. In order to correct the catalytic activity considering the surface area, the last column in Table 1 presents the specific constant rate normalized by S_{BET}. The sample with 0.02 mol% Pt had the highest value for this parameter. In this case, the normalized rate constant is about 6.5 times higher than that of pure TiO_2. Additionally, for the best compositions, only around 5 min (Table 1) was necessary to reduce the dye concentration by half. Based on the data in Fig. 2, these modified catalysts required around 50 min less to decolorate the MO solution when compared to pure TiO_2.

Fig. 3 shows the XRD patterns of TiO_2 and of Pt-TiO_2 powders. The Pt amount increase led to a significant variation in the catalyst structure. Pure TiO_2 sample is composed only by anatase phase. For those samples modified with Pt, a small amount of rutile had also

Table 1
Apparent rate constant, k, half life time, surface area and k normalized by area values.

Nominal Pt concentration (mol%)	$k \times 10^{-2}$ (min^{-1})	$t_{1/2}$ (min)	S_{BET} (m^2 g^{-1})	$k/S_{BET} \times 10^{-4}$ (g min^{-1} m^{-2})
0	3.10	22.3	76.2	4.07
0.005	7.34	9.4	53.6	13.7
0.01	7.62	9.1	58.3	13.1
0.02	10.2	6.8	39.3	26.0
0.05	11.3	6.1	52.0	21.8
0.1	11.1	6.3	48.6	22.7
0.2	12.8	5.4	52.8	24.2
1.0	11.4	6.1	84.7	13.4
5.0	11.3	6.1	60.9	18.6
10.0	9.89	7.0	64.4	15.4
P25	3.59	19.3	50.0	7.18

Table 2
Structural compositions determined by the Rietveld refinement for Pt-loaded TiO_2 catalysts.

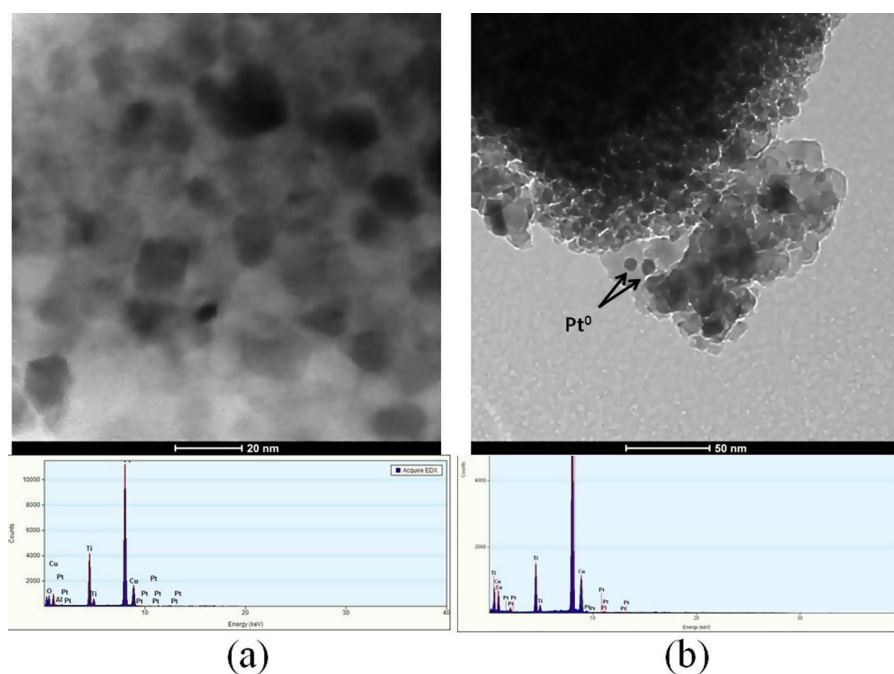| Nominal Pt concentration (mol%)	Anatase (%)	Rutile (%)	Pt^0 (%)
0	100 ± 1.0	–	–
0.005	97.9 ± 1.0	2.1 ± 1.0	–
0.01	97.1 ± 1.0	2.9 ± 1.0	–
0.02	98.7 ± 1.0	1.3 ± 1.0	–
0.05	98.1 ± 1.0	1.9 ± 1.0	–
0.1	99.3 ± 1.0	0.70 ± 1.0	–
0.2	97.8 ± 1.0	2.2 ± 1.0	–
1.0	97.2 ± 1.0	1.3 ± 1.0	1.5 ± 1.0
5.0	93.8 ± 1.0	0.80 ± 1.0	5.4 ± 1.0
10.0	87.9 ± 1.0	2.0 ± 1.0	10.1 ± 1.0

Fig. 4. TEM images and EDX analysis of Pt-TiO$_2$ samples: (a) (Pt 0.05%)TiO$_2$ and (b) (Pt 0.1%)TiO$_2$.

been detected (Table 2). Such results have also been described in the literature for Ag-doped TiO$_2$ prepared by the sol–gel process [38], and for Pt-TiO$_2$ prepared by Sánchez et al. [39] using sol–gel route and by Teoh et al. [40] using flame spray pyrolysis process. Using the Rietveld refinement procedure it was possible to calculate the quantitative data from the diffractograms, which are presented in Table 2. The data also show the cubic phase peak relates to metallic Pt for 1, 5, and 10% Pt-TiO$_2$ samples, which occurs at $2\theta = 39.8°$. However, TEM analysis shows that the beginning of segregation of Pt metal phase occurs around 0.1 mol%. In Fig. 4, for 0.05 mol% Pt sample, only TiO$_2$ crystalline planes are observed with a particle size distribution between 10 and 20 nm, indicating that at this Pt-loading, the Pt ions where incorporated into the TiO$_2$ crystal lattice. On the other hand, TEM images and EDX analysis detected the presence of few and small Pt particles on the TiO$_2$ surface for the sample with 1 mol% Pt. The amount of Pt in this sample was too small to be detected by XRD analysis.

The lattice parameters present no significant change in the anatase phase, whereas for the rutile phase an increase of the parameters at 0.2 and 1.0 mol% of Pt-loading was observed, as shown in Fig. 5. Therefore, one possible explanation is that Pt introduction leads to a TiO$_2$ partial phase transition, from anatase to rutile, and the Pt atoms are incorporated in this latter phase. Such proposition also supports the relaxation of the rutile phase lattice parameters for Pt-loading higher than 1 mol%, which could be related to Pt-phase segregation. As can be seen in Fig. 6, Pt-loading at low levels (<0.1 mol%) produces an increase in the average crystallite size for both phases, anatase and rutile. However, this effect is more pronounced in the rutile phase. This fact could explain the decrease in the specific surface area data. It is important to remember that the photoactivity of pure TiO$_2$ is dependent on different variables, such as surface area, anatase/rutile proportion, crystallite size, and surface states. The results presented here allow us to propose that small amounts of Pt by itself can induce important changes in the photocatalytic properties of the oxide.

Considering the results presented above, there are two possibilities to explain the changes in the photocatalyst properties. The first

occurs by the doping process, where platinum ions could replace Ti^{4+} ions in the crystal lattice, according to the following equation (using Kröger and Vinck notation):

$$PtO \xrightarrow{TiO_2} Pt''_{Ti} + 2O^x_O + V^{\bullet\bullet}_O \qquad (2)$$
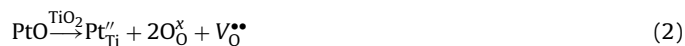
in which the main symbol indicates the defect species, the subscript symbol determines its localization in the lattice (in this case, Pt defects are substitutional), and the superscript symbol indicates the charge of the defect in relation to the perfect lattice. Considering the charge of the perfect crystal, positive charges are denoted by a dot, negative charges by a comma, and neutral defects by an x. For example, $V^{\bullet\bullet}_O$ is a doubly positively charged oxygen vacancy. Considering that TiO$_2$ is an n-type semiconductor, the introduction of Pt''_{Ti} defects generates more negatively charged carriers. Moreover, the introduction of Pt ions also has a secondary effect; the
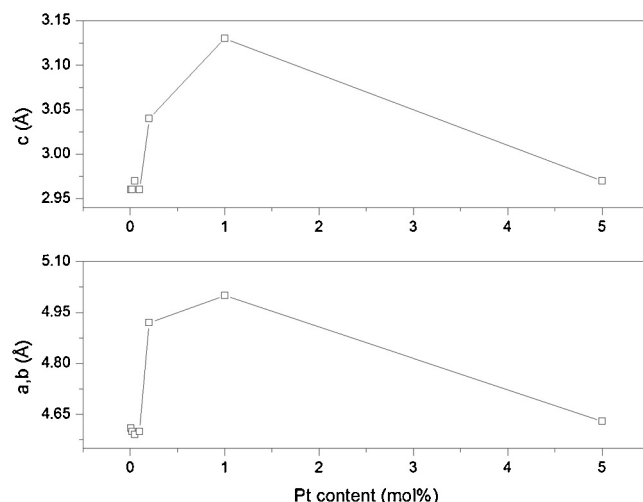

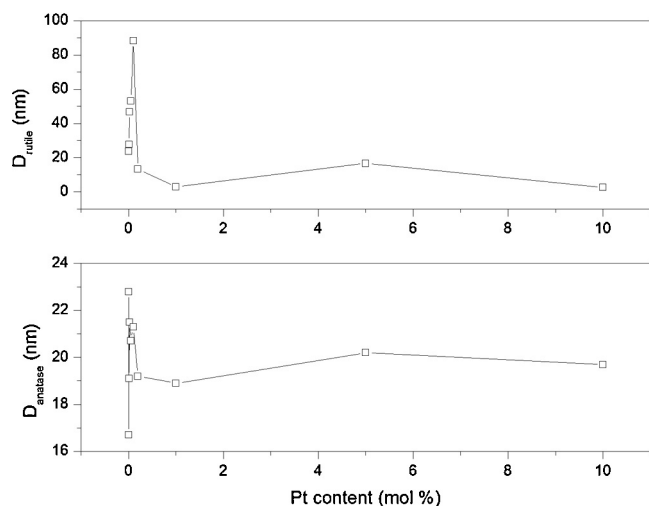**Fig. 5.** Rutile lattice parameters variation as a function of Pt-loading.

Fig. 6. Crystallite size variation as a function of Pt-loading.

Fig. 7. TEM image of (Pt 5.0%)TiO$_2$ sample.

formation of the TiO$_2$ rutile phase, which is described as enhancing the photocatalytic properties of the oxide due to formation of solid–solid interface [41–44]. A combination of both effects, the increase of the charge carrier density and the formation of rutile TiO$_2$, could be an explanation for the enhancement of photocatalytic properties presented here.

On the other hand, if the Pt amount exceeds the concentration limit for solid solution formation, phase segregation occurs. In this case, Pt clusters are expelled from the bulk to the surface of the TiO$_2$ particles due to its higher density than that of TiO$_2$. As described by Linsebigler et al. [45], a Schottky barrier is formed between metal and semiconductor interfaces, and Fermi levels are equilibrated. After irradiation, conduction band electrons of TiO$_2$ flow to the Pt sites. Therefore, the Schottky barrier acts as an efficient electron trap and decreases the rate of e$^-$/h$^+$ pair recombination. Moreover, platinum can act as a reducing site, leading to an increase in photoactivity. It is clear that the key to maximum photocatalytic activity in metal-decorated semiconductors is the contact between the two phases, which depends on the preparation method. In contrast to Pt photodeposition methods [29–31], which are widely used, the synthesis method used in this study, produced Pt particles of much higher size than those produced by the first methods (10–20 nm versus 2 nm), which could be a disadvantage. However, the Pt-loading was low enough to ensure a large exposed surface area of TiO$_2$. Besides, the polymeric precursor method allowed close contact between the two phases and also a homogeneous distribution of Pt clusters throughout the catalyst, as shown in Fig. 7 for the sample with 5 mol% Pt. Linsebigler et al. [45] also discussed that the Pt cluster size and morphology do not have important roles regarding the photocatalytic properties. The authors propose that there is a metal concentration limit above which the photocatalytic efficiency decreases, due to it exceeding an optimal level of electron distribution on the surface. In our case, for those samples where there is phase segregation, we observed that the k value decreased for 5 and 10 mol% loaded samples, which is in agreement with the proposition of Linsebigler et al. [45].

Summarizing, our results indicate different behaviours for Pt-modified TiO$_2$ using a one-step procedure: first, for samples at the doping level region, and second for samples at the Pt-phase segregation. The photocatalytic results of doped and platinized samples denote that both procedures result in significant improvement of the photoactivity of TiO$_2$ under UV irradiation. No significant differences were observed in terms of the discoloration of methyl orange on doped or metalized TiO$_2$ samples. If we consider the additional cost of Pt, it is clear that the doping procedure presents advantages.
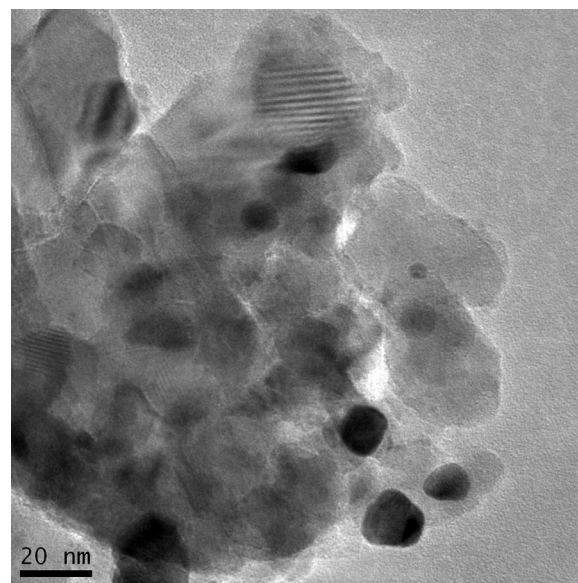
Additionally, the highest photocatalytic activities were obtained with doped samples when compared to the metallized samples.

4. Conclusions

Pt-TiO$_2$ nanoparticles were successfully prepared by the polymer precursor method. This method proved to be a simple and low-cost process to prepare TiO$_2$ photocatalysts with refined control of its properties. The specific surface areas of Pt-doped TiO$_2$ were in the range of 48–84 m^2 g^{-1}. All Pt-loaded materials presented improved photoactivity when compared to pure TiO$_2$. XRD patterns showed that platinum ions could be incorporated into the TiO$_2$ lattice at low Pt content levels, followed by the conversion of small portions of anatase in the rutile phase. Otherwise, if Pt content values of more than 0.1 mol% are used, a metal Pt phase segregates onto the TiO$_2$. However, almost no difference was observed in the photoactivity when doped samples and metallized samples were compared. In doped samples the enhancement on the photocatalytic activity should be related to the creation of electronic defects coupled to the presence of small amounts of rutile phase. For metalized samples, this improvement is probably due to a separation of charges, preventing in this sense, the recombination of charge carriers, electrons and holes. These results clearly demonstrate that TiO$_2$ doped with low concentrations of Pt ions is a promising material as well as the platinized TiO$_2$.

References

[1] V.G. Bessergenev, R.J.F. Pereira, M.C. Mateus, I.V. Khmelinskii, D.A. Vasconcelos, R. Nicula, E. Burkel, A.M. Botelho do Rego, A.I. Saprykin, Thin Solid Films 503 (2006) 29–39.
[2] H. Sun, C. Wang, S. Pang, X. Li, Y. Tao, H. Tang, M. Liu, J. Non-Cryst. Solids 354 (2008) 1440–1443.
[3] K.-H. Wang, Y.-H. Hsieh, T.-T. Lin, C.-Y. Chang, React. Kinet. Catal. Lett. 95 (2008) 39–46.
[4] F.J. Ager, I. Justicia, R. Gerbasi, G.A. Battiston, N. McSporran, A. Figueras, Nuclear Instrum. Methods Phys. Res. B 249 (2006) 490–492.
[5] R.D. Duminica, F. Maury, R. Hausbrand, Surf. Coat. Technol. 201 (2007) 9349–9353.

[6] B. Cojocaru, S. Neatu, E. Sacaliuc-Parvulescu, F. Levy, V.I. Parvulescu, H. Garcia, Appl. Catal. B: Environ. 107 (2011) 140–149.
[7] K. Eufinger, E.N. Janssen, H. Poelman, D. Poelman, R. De Gryse, G.B. Marin, Thin Solid Films 515 (2006) 425–429.
[8] B. Liu, Q.H.L. Wen, X. Zhao, Thin Solid Films 517 (2009) 6569–6575.
[9] K.Y. Jung, S.B. Park, H.D. Jang, Catal. Commun. 5 (2004) 491–497.
[10] R. Kavitha, S. Meghani, V. Jayaram, Mater. Sci. Eng. B: Solid State Mater. Adv. Technol. 139 (2007) 134–140.
[11] S.R. Dhage, R. Pasricha, V. Ravi, Mater. Res. Bull. 38 (2003) 1623–1628.
[12] N.R. Mathews, E.R. Morales, M.A. Cortés-Jacome, J.A. Toledo Antônio, Sol. Energy 83 (2009) 1499–1508.
[13] K. Prasad, D.V. Pinjari, A.B. Pandit, S.T. Mhaske, Ultrason. Sonochem. 17 (2010) 409–415.
[14] L. Lopez, W.A. Daoud, D. Dutta, Surf. Coat. Technol. 205 (2010) 251–257.
[15] G.K. Mor, O.K. Varghese, M. Paulose, K. Shankar, C.A. Grimes, Sol. Energy Mater. Sol. Cells 90 (2006) 2011–2075.
[16] J.M. Macak, H. Tsuchiya, A. Ghicov, K. Yasuda, R. Hahn, S. Bauer, P. Schmuki, Curr. Opin. Solid State Mater. Sci. 11 (2007) 3–18.
[17] K. Onoda, S. Yoshikawa, J. Solid State Chem. 180 (2007) 3425–3433.
[18] H.-C. Liang, X.-Z. Li, J. Hazard. Mater. 162 (2009) 1415–1422.
[19] K. Lee, D. Kim, P. Roy, I. Paramasivam, B.I. Birajdar, E. Spiecker, P. Schmuki, J. Am. Ceram. Soc. 132 (2010) 1478–1479.
[20] M.S. Sikora, A.V. Rosario, E.C. Pereira, C.O. Paiva-Santos, Electrochim. Acta 56 (2011) 3122–3127.
[21] M.C. Hidalgo, M. Aguiar, M. Maicu, J.A. Navío, G. Cólon, Catal. Today 129 (2007) 50–58.
[22] K.V. Baiju, S. Shukla, S. Biju, M.L.P. Reddy, K.G.K. Warrier, Catal. Lett. 131 (2009) 663–671.
[23] O. Carp, C.L. Huisman, A. Reller, Prog. Solid State Chem. 32 (2004) 33–177.
[24] S. Rehman, R. Ullah, A.M. Butt, N.D. Gohar, J. Hazard. Mater. 170 (2009) 560–569.
[25] T. Lana-Villarreal, R. Gómez, Electrochem. Commun. 7 (2005) 1218–1224.
[26] F. Zhang, R. Jin, J. Chen, C. Shao, W. Gao, L. Li, N. Guan, J. Catal. 232 (2005) 424–431.
[27] S. Oros-Ruiz, J.A. Pedraza-Avella, C. Gusmán, M. Quintana, E. Moctezuma, G. del Angel, R. Gómez, E. Pérez, Top. Catal. 54 (2011) 519–526.
[28] S.W. Lam, K. Chiang, T.M. Lim, R. Amal, G.K.-C. Low, Appl. Catal. B: Environ. 72 (2007) 363–372.
[29] D. Hufschmidt, D. Bahnemann, J.J. Testa, C.A. Emilio, M.I. Litter, J. Photochem. Photobiol. A: Chem. 148 (2002) 223–231.
[30] M.C. Hidalgo, M. Maicu, J.A. Navío, G. Colón, Appl. Catal. B: Environ. 81 (2008) 49–55.
[31] T.A. Egerton, J.A. Mattinson, J. Photochem. Photobiol. A: Chem. 194 (2008) 283–289.
[32] C.-H. Huang, J.-K. Wang, Y.-M. Lim, Y.-H. Tseng, C.-M. Lu, J. Mol. Catal. A: Chem. 316 (2010) 163–170.
[33] S. Ymazaki, Y. Fujiwara, S. Yabuno, K. Adachi, K. Honda, Appl. Catal. B: Environ. 121–122 (2012) 148–153.
[34] B.K. Vijayan, N.M. Dimitrijevic, J. Wu, K.A. Gray, J. Phys. Chem. C 114 (2010) 21262–21269.
[35] J. Choi, H. Park, M.R. Hoffmann, J. Phys. Chem. C 114 (2010) 783–792.
[36] S. Kim, S.-J. Hwang, W. Choi, J. Phys. Chem. B 109 (2005) 24260–24267.
[37] A.C. Larson, R.B. Von Dreele, General Structure Analysis System (GSAS), Los Alamos National Laboratory Report, LAUR, 2000, pp. 86–748.
[38] H.E. Chao, Y.U. Yun, H.U. Xingfang, A. Larbot, J. Eur. Ceram. Soc. 23 (2003) 1457–1464.
[39] E. Sánchez, T. López, R. Gómez, Bokhimi, A. Morales, O. Novaro, J. Solid State Chem. 122 (1996) 309–314.
[40] W.Y. Teoh, L. Mädler, D. Beydoun, S.E. Pratsinis, R. Amal, Chem. Eng. Sci. 60 (2005) 5852–5861.
[41] K.M. Schindler, M. Kunst, J. Phys. Chem. 94 (1990) 8222–8226.
[42] T. Miyagi, M. Kamei, T. Mitsuhashi, T. Ishigaki, A. Yamazaki, Chem. Phys. Lett. 390 (2004) 399–402.
[43] D.C. Hurum, A.G. Agrios, K.A. Gray, T. Rajh, M.C. Thurnauer, J. Phys. Chem. B 107 (2003) 4545–4549.
[44] G. Li, K.A. Gray, Chem. Phys. 339 (2007) 173–187.
[45] A.L. Linsebigler, G. Lu, J.T. Yates Jr., Chem. Rev. 95 (1995) 735–758.